

UNCLASSIFIED

AD NUMBER

AD329345

CLASSIFICATION CHANGES

TO: unclassified

FROM: confidential

LIMITATION CHANGES

TO:  
Approved for public release, distribution unlimited

FROM:  
Distribution authorized to U.S. Gov't. agencies and their contractors; Administrative/Operational Use; MAY 1962. Other requests shall be referred to Air Force Arnold Engineering Development Center, Arnold AFB, TN.

AUTHORITY

AEDC USAF ltr, 12 Feb 1973; AEDC, USAF ltr, 12 Feb 1973

THIS PAGE IS UNCLASSIFIED

**AD 329 345**

*Reproduced  
by the*

**ARMED SERVICES TECHNICAL INFORMATION AGENCY  
ARLINGTON HALL STATION  
ARLINGTON 12, VIRGINIA**



NOTICE: When government or other drawings, specifications or other data are used for any purpose other than in connection with a definitely related government procurement operation, the U. S. Government thereby incurs no responsibility, nor any obligation whatsoever; and the fact that the Government may have formulated, furnished, or in any way supplied the said drawings, specifications, or other data is not to be regarded by implication or otherwise as in any manner licensing the holder or any other person or corporation, or conveying any rights or permission to manufacture, use or sell any patented invention that may in any way be related thereto.

AEDC-TDR-62-99

~~CONFIDENTIAL~~

ARO, INC.  
DOCUMENT CONTROL

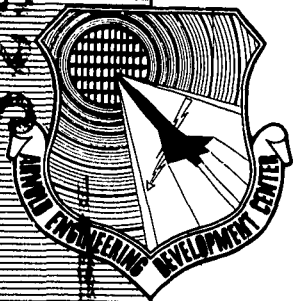
NO IG-237-343

COPY 52 OF 103

SERIES A PAGES 34

CLASSIFIED BY AS AD NO. 329345

329 345



(TITLE UNCLASSIFIED)

# THE AERODYNAMIC CHARACTERISTICS OF A 75-DEG SWEEP DELTA WING AT HIGH ANGLES OF ATTACK AND MACH NUMBERS OF 2 TO 8

By

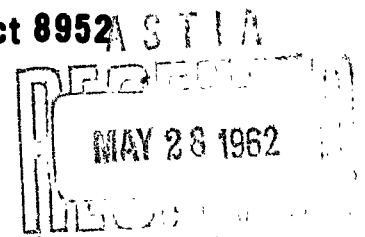
E. L. Clark and C. J. Spurlin

von Kármán Gas Dynamics Facility  
ARO, INC.

TECHNICAL DOCUMENTARY REPORT NO. AEDC-TDR-62-99

May 1962

AFSC Program Area 750A, Project 8952



(Prepared under Contract No. AF 40(600)-800 S/A 24(61-73) by ARO, Inc.,  
contract operator of AEDC, Arnold Air Force Station, Tennessee.)

**ARNOLD ENGINEERING DEVELOPMENT CENTER**

**AIR FORCE SYSTEMS COMMAND**

**UNITED STATES AIR FORCE**

DOWNGRADED AT 3 YEAR INTERVALS;  
DECLASSIFIED AFTER 12 YEARS.  
DOD DIR 5200.10

~~CONFIDENTIAL~~

(Title Unclassified)

THE AERODYNAMIC CHARACTERISTICS  
OF A 75-DEG SWEPT DELTA WING AT HIGH  
ANGLES OF ATTACK AND MACH NUMBERS OF 2 TO 8

By

E. L. Clark and C. J. Spurlin

von Kármán Gas Dynamics Facility

ARO, Inc.

a subsidiary of Sverdrup and Parcel, Inc.

May 1962

ARO Project No. 933002

~~CONFIDENTIAL~~

(This abstract is UNCLASSIFIED.)

#### ABSTRACT

An experimental investigation has been conducted in the 12-in. Supersonic Tunnel and the 50-in. Mach 8 Tunnel of the von Kármán Gas Dynamics Facility to determine the aerodynamic characteristics of a delta wing at high angles of attack. The configuration tested was a flat, blunt leading edge, delta wing with 75-deg sweepback. The tests were conducted at angles of attack from 30 to 105 deg and Mach numbers of 2, 3, 5, and 8. Longitudinal stability and drag characteristics, surface pressure distributions, and shock wave shapes are presented with theoretical estimates based on the Newtonian theory.

## CONTENTS

	<u>Page</u>
ABSTRACT . . . . .	iii
NOMENCLATURE . . . . .	vii
1.0 INTRODUCTION . . . . .	1
2.0 APPARATUS AND TEST PROCEDURE	
2.1 Wind Tunnels . . . . .	1
2.2 Models and Supports . . . . .	2
2.3 Instrumentation and Data Accuracy . . . . .	2
2.4 Test Conditions . . . . .	3
3.0 RESULTS AND DISCUSSION	
3.1 Shock Wave Geometry . . . . .	3
3.2 Longitudinal Stability and Drag Characteristics . . . . .	4
3.3 Pressure Distribution . . . . .	5
4.0 CONCLUSIONS . . . . .	7
REFERENCES . . . . .	7

## ILLUSTRATIONS

Figure

1. Wind Tunnels	
a. The 12-in. Supersonic Tunnel . . . . .	9
b. The 50-in. Mach 8 Tunnel . . . . .	10
2. Model Details . . . . .	11
3. Photograph of Small Model and Support . . . . .	11
4. Shadowgraph Pictures of the Model at $M_\infty = 8$ and Various Angles of Attack . . . . .	12
5. Schlieren Picture of the Model at $M_\infty = 5$ and $\alpha = 45$ deg . . . . .	13
6. Longitudinal Stability and Drag Characteristics	
a. Axial Force, $M_\infty = 8$ . . . . .	14
b. Normal Force . . . . .	14
c. Center of Pressure, $M_\infty = 8$ . . . . .	15
d. Pitching Moment . . . . .	15
e. Lift . . . . .	16
f. Drag . . . . .	17
g. Lift-to-Drag Ratio . . . . .	17

<u>Figure</u>	<u>Page</u>
7. Effect of Mach Number on the Pitch-Up Angle of Attack . . . . .	18
8. Pressure Distribution on Model Center- line, $M_\infty = 8$ . . . . .	19
9. Effect of Angle of Attack on Centerline Pressure, $M_\infty = 8$ . . . . .	20
10. Lateral Pressure Distribution at $x/l = 0.51$ , $M_\infty = 8$ . . . . .	21
11. Local Normal-Force Distribution, $M_\infty = 8$ . . . . .	22
12. Local Pitching-Moment Distribution, $M_\infty = 8$ . . . . .	23
13. Pressure Distribution on Model Centerline, $M_\infty = 2$ . . . . .	24
14. Effect of Angle of Attack on Centerline Pres- sure, $M_\infty = 2$	
a. Windward . . . . .	25
b. Leeward . . . . .	25
15. Schlieren Pictures of the Wake Geometry at $M_\infty = 2$ . . . . .	26



## NOMENCLATURE

$b'$	Local model semi-span
$C_A$	Forebody axial-force coefficient, forebody axial force/ $q_\infty S$
$C_D$	Drag coefficient, drag/ $q_\infty S$
$C_L$	Lift coefficient, lift/ $q_\infty S$
$C_m$	Pitching-moment coefficient referenced to $0.6\ell$ , pitching moment/ $q_\infty S \bar{c}$ or $\int_0^1 C_m' d(x/\ell)$
$C_m'$	Local pitching-moment coefficient, $\frac{\ell}{\bar{c}} (0.6 - x/\ell) C_N'$
$C_N$	Normal-force coefficient, normal force/ $q_\infty S$ or $\int_0^1 C_N' d(x/\ell)$
$C_N'$	Local normal-force coefficient, $\frac{2\ell b'}{S} \int_0^1 (C_{P_{\text{lower surface}}} - C_{P_{\text{upper surface}}}) d(y/b')$
$C_p$	Pressure coefficient, $(p - p_\infty)/q_\infty$
$\bar{c}$	Mean aerodynamic chord
$L/D$	Lift-to-drag ratio
$\ell$	Model length (root chord)
$M_\infty$	Free-stream Mach number
$p$	Surface pressure
$p_\infty$	Free-stream static pressure
$q_\infty$	Free-stream dynamic pressure
$Re$	Free-stream Reynolds number based on model length
$S$	Wing planform area
$T_0$	Free-stream stagnation temperature
$x$	Longitudinal distance measured from model nose
$x_{cp}/\ell$	Longitudinal distance from model nose to center of pressure, $(C_m/C_N) (\bar{c}/\ell) + 0.6$
$y$	Lateral distance measured from model centerline
$\alpha$	Angle of attack

$\alpha_p$  Pitch-up angle of attack (The angle of attack at which the pitching moment derivative,  $dC_m/d\alpha$ , is essentially discontinuous.)

$\eta$  Angle between free-stream velocity and unit vector normal to model surface

Note: Model geometry parameters,  $b'$ ,  $\bar{c}$ ,  $l$ ,  $S$ ,  $x$ , and  $y$  are defined in Fig. 2.

## 1.0 INTRODUCTION

Winged vehicles which can produce lift during re-entry have certain advantages over a vehicle which follows a ballistic trajectory. These advantages include increased range and maneuverability, reduced peak deceleration, and improved landing characteristics. The maximum heating rate and total heat load for which such a hypersonic glider must be designed can be significantly reduced by having the vehicle enter the earth's atmosphere at a large angle of attack, thereby providing a high drag, low L/D re-entry. This type of maneuver requires the glider to fly near maximum lift over a large portion of the re-entry trajectory. As a result of this requirement there has been considerable interest in the aerodynamic characteristics of delta wings at high angles of attack.

Studies (Refs. 1 through 5) indicate that delta wing configurations. The purpose of the present investigation was to determine the effects of Mach number and high angles of attack on the longitudinal stability of a delta wing and to study in detail the pitch-up tendency at angles of attack near maximum lift. Static force measurements were used to obtain the drag and stability characteristics of the wing, and pressure measurements were utilized to determine the local load distribution. Theoretical estimates of the characteristics, based on the Newtonian theory, are presented with the data.

The tests were conducted in the von Kármán Gas Dynamics Facility of the Arnold Engineering Development Center (VKF-AEDC), Air Force Systems Command (AFSC). Measurements were made in the 12-in. Supersonic Tunnel and the 50-in. Mach 8 Tunnel at nominal Mach numbers of 2, 3, 5, and 8, free-stream Reynolds numbers of 0.31 to  $1.57 \times 10^6$  based on model length, and angles of attack from 30 to 105 deg.

## 2.0 APPARATUS AND TEST PROCEDURE

### 2.1 WIND TUNNELS

The 12-in. Supersonic Tunnel (Fig. 1a) is an intermittent, variable-density wind tunnel with a manually adjusted, flexible-plate-type nozzle.

---

Manuscript released by authors April 1962.

The tunnel operates at Mach numbers from 1.5 to 5, at stagnation pressures from about 1 to 60 psia, and at stagnation temperatures up to about 80°F.

The 50-in. Mach 8 Tunnel (Fig. 1b) is an axisymmetric, continuous-flow, variable-density wind tunnel. The tunnel operates at stagnation pressures from 100 to 800 psia and at a maximum stagnation temperature of 900°F.

A complete description of the tunnels is given in Ref. 6.

## 2.2 MODELS AND SUPPORTS

The test configuration (Fig. 2) was a flat or slab delta wing with a 75-deg sweepback angle. The cylindrically blunted leading edges intersected to give a sharp-nosed planform. As is shown in Fig. 2, two model sizes were used. The large model was tested in the 50-in. tunnel, and the small model was tested in the 12-in. tunnel. After the force tests were completed, both models were modified for the pressure tests by installing pressure orifices on the lower surface of the wing.

Support interference was minimized by mounting the models at an angle to the balance as shown in the photograph of the small model (Fig. 3). Because very high angles of attack were obtained in the hypersonic tests, the model used in these tests was mounted at an angle of 90 deg to the balance axis. The tunnel sector angle range of 30 deg was augmented with various bent stings to provide angles of attack from 30 to 105 deg. For the supersonic tests a model-balance angle of 45 deg was used with a 15-deg bent sting to give angles of attack from 25 to 65 deg. The pressure models were supported in a similar manner.

## 2.3 INSTRUMENTATION AND DATA ACCURACY

Two six-component, internal, strain-gage balances were used to measure the aerodynamic forces and moments on the models. Surface pressures were measured with variable reluctance transducers referenced to a monitored pressure.

Estimated accuracy of the coefficients is given in the following table:

$\frac{C_N}{\pm 0.020}$	$\frac{C_m}{\pm 0.004}$	$\frac{C_A}{\pm 0.002}$	$\frac{C_p}{\pm 0.015}$
-------------------------	-------------------------	-------------------------	-------------------------

Accuracy of the angle of attack is  $\pm 0.2$  deg.

## 2.4 TEST CONDITIONS

The tests were conducted at the following tunnel conditions:

<u>M<sub>∞</sub></u>	<u>Re x 10<sup>-6</sup></u>	<u>T<sub>0</sub>, °R</u>
2.00	0.31	540
2.99	0.38	540
5.01	0.74	540
8.05	1.57	1280

## 3.0 RESULTS AND DISCUSSION

The aerodynamic characteristics of the wing were calculated using Newtonian impact theory, and the results are presented with the experimental data. Newtonian theory gives the pressure coefficient on windward surfaces as  $C_p = 2 \cos^2 \eta$  where  $\eta$  is the angle between the free-stream velocity vector and a unit vector normal to the surface. The inclusion of centrifugal corrections is not considered here because only the leading edges are curved, and they contribute a minor part of the wing stability. It has been suggested that a modified form of the Newtonian theory with the coefficient 2 replaced by  $C_{p_{max}}$  should be used for surfaces with detached shock waves. However, as will be shown, the surface pressures on a delta wing with detached shock cannot be predicted as a function of surface inclination only.

### 3.1 SHOCK WAVE GEOMETRY

The flow over a highly swept delta wing is essentially conical for angles of attack between 30 deg and the shock detachment angle (Ref. 7). Therefore, the angle of attack at which shock detachment occurs on a delta wing should be closely approximated by the theoretical cone angle for shock detachment as given in Ref. 8. This hypothesis is substantiated by Mach 8 shadowgraph pictures such as those shown in Fig. 4. The shock wave is straight for angles of attack less than 57 deg. When the angle of attack is increased above 57 deg, the shock develops increasing curvature near the model nose and trailing edge. This curvature of the shock wave is considered to be an indication of shock detachment. Thus, the delta wing shock detachment angle of attack measured at Mach 8 (57 deg) agrees well with the theoretical cone semivertex angle required for shock detachment (56.3 deg at  $M_\infty = 8$ ). It is assumed that this agreement holds for lower Mach numbers, and the conical shock detachment angle plotted in Fig. 7 will be used as an indication of the delta wing, shock detachment angle.

A schlieren photograph of the model at Mach 5 and  $\alpha = 45$  deg is shown in Fig. 5. For these conditions where the shock is attached, there is a Prandtl-Meyer expansion flow at the wing trailing edge.

### 3.2 LONGITUDINAL STABILITY AND DRAG CHARACTERISTICS

The longitudinal stability and drag characteristics of the model are presented in Fig. 6. Forebody axial force and center-of-pressure location are given only for Mach 8 because of inaccuracies which were introduced during the supersonic tests in resolving the balance forces through the model-balance angle. The conical shock detachment angle is indicated on the curves of Fig. 6 by vertical arrows. At angles of attack less than the angle for shock detachment the characteristics are similar for all test Mach numbers and show the usual decrease in magnitude as the Mach number is increased. However, as the shock detachment angle is reached at each Mach number there is a forward movement of the center of pressure (as shown in Fig. 6c for Mach 8), resulting in an abrupt, almost discontinuous, change in the pitching-moment derivative,  $dC_m/d\alpha$ .

At Mach 2 there is a sudden decrease in normal force at  $\alpha = 45$  deg which is about five degrees above the predicted detachment angle (Fig. 6b). A detailed discussion of this discontinuous behavior is given in section 3.3, Pressure Distribution.

The wind axis coefficients show similar trends. Since the axial force of the wing is small, the lift and drag are essentially vector components of the normal force. This is apparent in the lift-to-drag ratio (Fig. 6g), which is the same for all Mach numbers at angles of attack above 35 deg and is well represented by  $L/D = \cot \alpha$ .

With the exception of axial force, the theoretical estimates are in fair agreement with the Mach 8 measurements up to an angle of attack of about 55 deg. Above the shock detachment angle of attack, the simple theory cannot predict the aerodynamic characteristics.

The angle of attack at which the pitching-moment derivative,  $dC_m/d\alpha$ , changes abruptly is denoted as the "pitch-up angle of attack", and the effect of Mach number on this angle is shown in Fig. 7. As was mentioned in the Introduction, this behavior was observed in the data of Refs. 2 through 5 for configurations similar to that of the present test, and these data are included in Fig. 7. Correlation of the pitch-up angle of attack with shock detachment angle of attack is indicated in the figure by the agreement with a theoretical curve (Ref. 8) of cone semivertex angle required for

shock detachment. Data presented in Refs. 3 and 5 for delta wings with trailing edge control surfaces indicate that the pitch-up angle of attack is not strongly influenced by flap deflections of  $\pm 20$  deg.

### 3.3 PRESSURE DISTRIBUTION

Pressure distribution studies were made at Mach numbers of 2 and 8 to define the local aerodynamic conditions on the delta wing at high angles of attack.

The longitudinal pressure distribution on the model centerline at Mach 8 is presented in Fig. 8. The lee side pressure coefficient varied from 0 to 0.01 over the angle of attack range of 30 to 105 deg. At angles of attack less than the shock detachment angle, the flow outside of the boundary layer on the windward side is supersonic, and there is a Prandtl-Meyer expansion at the trailing edge. Thus, if there were no boundary layer, the flow on the windward surface could expand to the low pressure of the lee side without producing a pressure gradient along the surface. The data at  $\alpha = 45$  deg (attached shock) show that the distribution along the centerline is essentially flat except for a small gradient near the trailing edge. This gradient is caused by the combined effects of a reduction in boundary layer thickness which changes the "effective" body shape and a flow of high pressure air through the subsonic portion of the boundary layer to the lee side. As the angle of attack is increased above the shock detachment angle, the flow behind the shock wave becomes subsonic. Then, the flow on the windward surface of the wing resembles the potential flow over a cone in a uniform subsonic stream with free-stream velocity similar to the velocity behind the shock. The flow accelerates towards the trailing edge with an accompanying negative pressure gradient as shown for  $\alpha = 60$  and 75 deg in Fig. 8. A sonic line occurs at the trailing edge and is followed by a Prandtl-Meyer expansion. At  $\alpha = 90$  deg the flow over the wing is essentially radial from a stagnation point on the centerline and is similar to the flow over a circular disk normal to the free stream (Ref. 7). At angles of attack above 90 deg the flow resembles the subsonic potential flow over a wedge with the wing trailing edge acting as a leading edge for the wedge.

Since the strong, negative, pressure gradient which occurs at angles of attack above the shock detachment angle is in a region of relatively large wing area, it produces the center-of-pressure movement which was observed in the stability characteristics (Fig. 6c). The abruptness of this change in the longitudinal pressure distribution is shown in Fig. 9 where the pressure at four wing stations is plotted versus angle of attack.

The simple Newtonian theory provides a fair estimate of the surface pressure until the shock detachment angle is reached (Fig. 9). At angles of attack near 90 deg the modified form of the Newtonian theory would give closer agreement with the pressure on the forward portion of the wing. However, for the presented wing stations the measured pressure does not reach a maximum at  $\alpha = 90$  deg as predicted by the theory. Therefore, even though there may be a wing station (probably near the wing centroid) where the pressure agrees with the theory in its modified form, no simple relation of pressure to local surface inclination could predict the pressure distribution at angles of attack above shock detachment.

The lateral distribution of pressure at Mach 8 is shown in Fig. 10 for wing station  $x/l = 0.51$  and is typical for all stations. Integration of these pressures at each station gives the local normal-force and pitching-moment coefficients as presented in Figs. 11 and 12. Forward of body station  $x/l = 0.8$  at  $\alpha = 45$  and 60 deg the local normal-force distribution is linear and agrees well with the theory. The effect of the longitudinal pressure gradient on normal force and pitching moment is apparent in these figures.

Longitudinal pressure distributions on the centerline of the model at Mach 2 are presented in Fig. 13. The shock detachment angle of attack is approximately 40 deg at this Mach number, and the data are very similar to the Mach 8 data near detachment. The effect of angle of attack on the surface pressure at Mach 2 is shown in Fig. 14. Again the trends of the windward side pressures are similar to those at Mach 8 except that the pressure does not change as abruptly at Mach 2.

As the angle of attack was increased from 45 to 48 deg at Mach 2, the lee side pressure increased from three-tenths of free-stream pressure to six-tenths as shown in Fig. 14b. This increase in upper surface pressure reduced the normal force of the wing as was shown in Fig. 6b. Since the pressure was constant over the upper surface, the pitching moment was not influenced by the change in pressure level. There was some hysteresis in the pressures as is shown in Fig. 14b. This hysteresis also appeared in the normal-force measurements at these angles of attack. Schlieren photographs (Fig. 15) show that there is a change in the wake geometry as the angle of attack is increased above 45 deg, and this is undoubtedly related to the rise in pressure level. The abrupt change in lee side pressure was not observed at the other test Mach numbers. A test at  $M_\infty = 2.5$  and angles of attack from 40 to 60 deg showed that for these conditions the lee side pressure was constant ( $0.3 p_\infty$ ), and there were no normal force discontinuities. Therefore, with the present test data, it cannot be determined whether this phenomenon is caused by support interference or is a valid result of delta wing wake flow at the low supersonic Mach number.



## 4.0 CONCLUSIONS

The results of an investigation of the aerodynamic characteristics of a 75-deg delta wing at high angles of attack and Mach numbers of 2 through 8 indicate the following conclusions:

1. The angle of attack for shock detachment on a highly swept delta wing is approximately the same as the cone semivertex angle for shock detachment at the same Mach number.
2. A strong longitudinal pressure gradient develops on the windward surface of a delta wing as the shock-detachment angle of attack is approached. This gradient causes a forward movement of the center of pressure with a resulting reduction of longitudinal stability. The angle of attack at which this occurs can be predicted from conical shock theory.
3. Newtonian theory gives fair agreement at hypersonic speeds with the measured centerline pressure distribution and longitudinal stability parameters of a delta wing with an attached shock wave. For angles of attack above shock detachment, the surface pressures cannot be obtained as a simple function of surface inclination.

1. ~~Penner, S. M., and Armstrong, William C., "Delta Wing Longitudinal Aerodynamic Characteristics at High Angles of Attack and High Mach Numbers,"~~

~~NASA Technical Memorandum, TM-X-1178, December 1960.~~

2. ~~Foster, R. L., "Longitudinal Aerodynamic Characteristics of a Delta Wing at High Angles of Attack,"~~

~~NASA Technical Memorandum, TM-X-1178, December 1960.~~

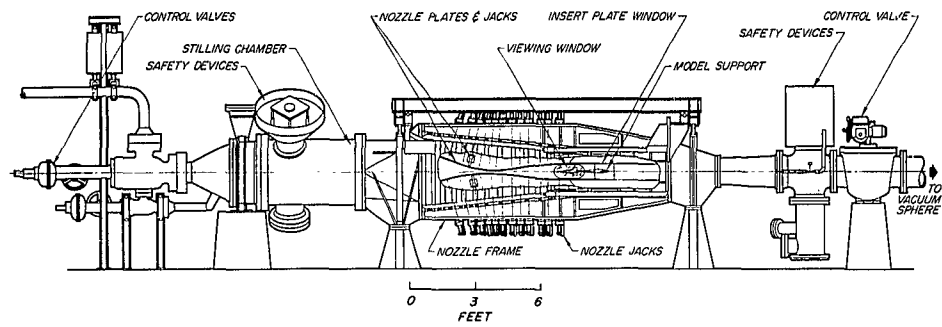
3. ~~Clark, J. C., "Longitudinal Aerodynamic and Stability Characteristics of a Delta Wing at High Angles of Attack,"~~

~~NASA Technical Memorandum, TM-X-338, December 1960.~~

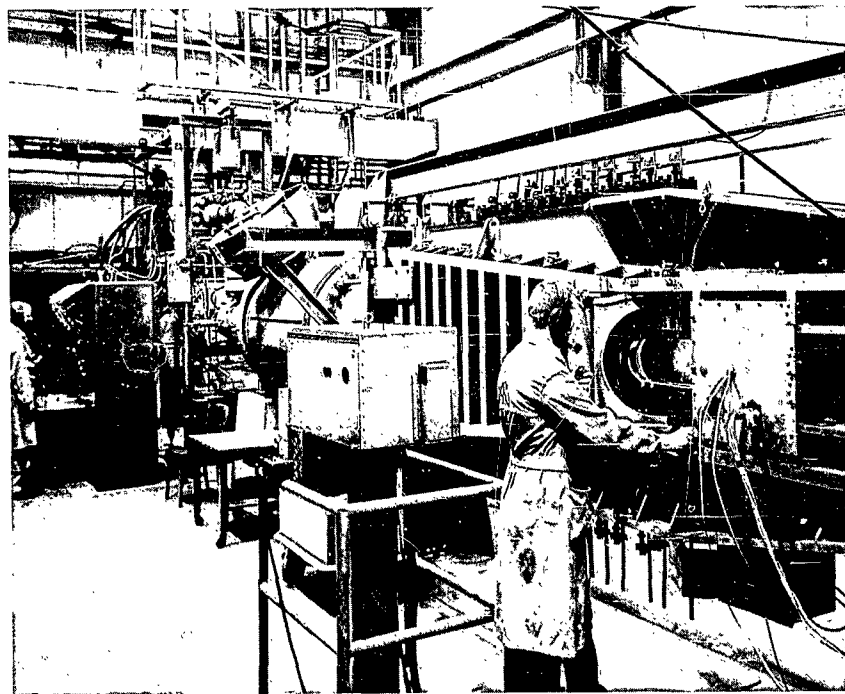
~~Clark, J. C., "Longitudinal Aerodynamic and Stability Characteristics of a Delta Wing at High Angles of Attack,"~~

~~NASA Technical Memorandum, TM-X-338, December 1960.~~

- ~~5. Wiggins, L. H. "Characteristics of Flow over a Thin Airfoil at High Angles of Incidence." AEDC-TDR-62-99. (Confidential)~~
6. Test Facilities Handbook, (3rd Edition). "von Kármán Gas Dynamics Facility, Vol. 4." Arnold Engineering Development Center, January 1961.
  7. Bertram, Mitchel H. and Henderson, Arthur, Jr. "Recent Hypersonic Studies of Wings and Bodies." ARS Journal, Vol. 31, No. 8, August 1961, pp 1129-1139.
  8. Ames Research Staff. "Equations, Tables, and Charts for Compressible Flow." NACA Report 1135, 1953.

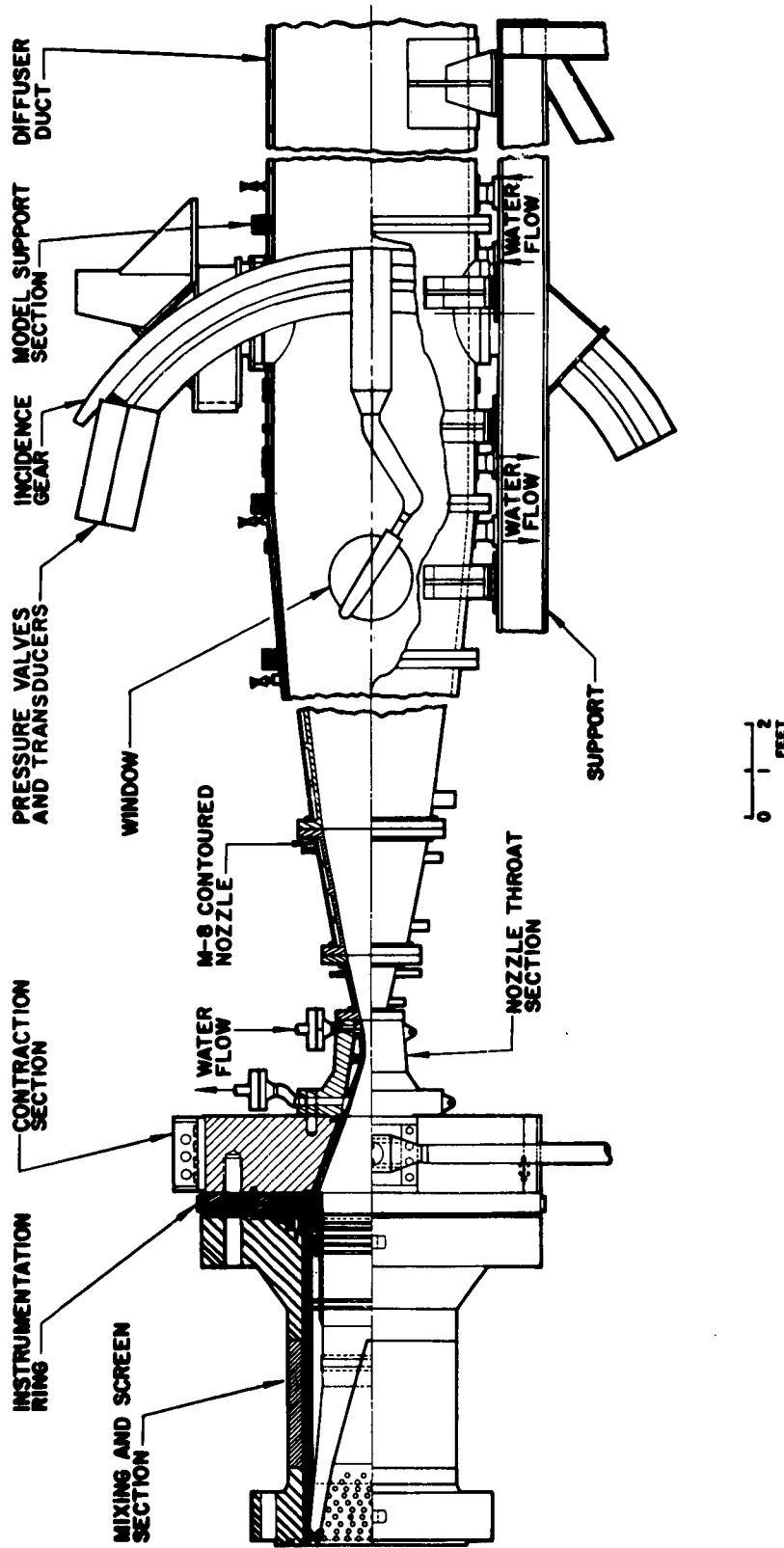


Assembly



a. The 12-in. Supersonic Wind Tunnel

Fig. 1 Wind Tunnels



b. The 50-in. Mach 8 Tunnel

Fig. 1 Concluded

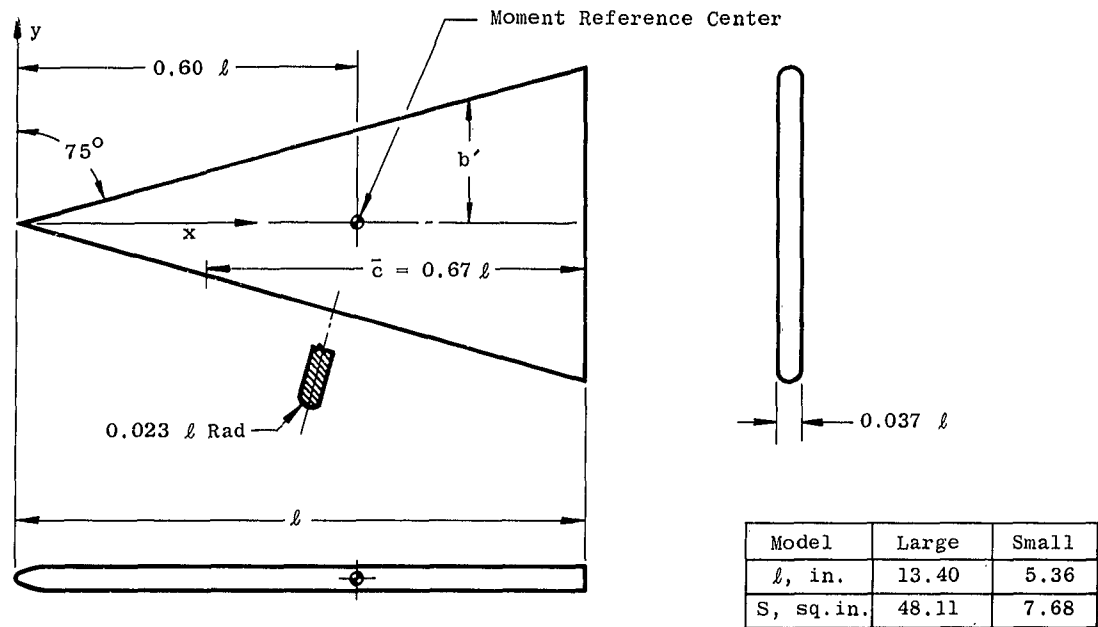
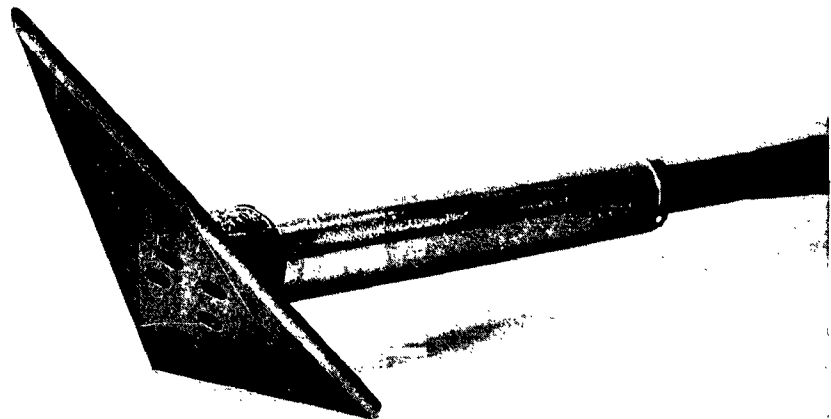


Fig. 2 Model Details

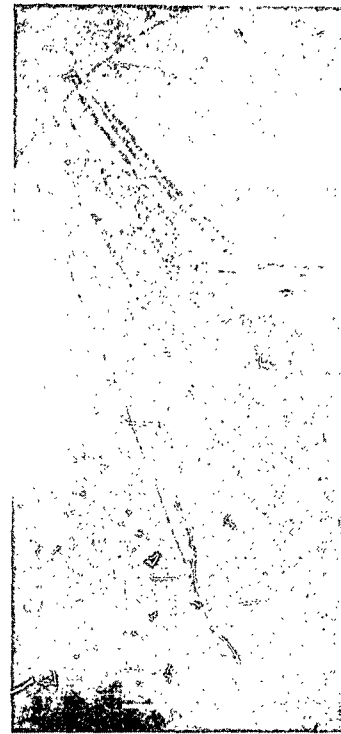


A E D C  
21563-U

Fig. 3 Photograph of Small Model and Support



$\alpha = 45^\circ$



$\alpha = 60^\circ$



$\alpha = 75^\circ$



$\alpha = 90^\circ$



$\alpha = 105^\circ$

Fig. 4 Shadowgraph Pictures of the Model at  $M_\infty = 8$  and Various Angles of Attack

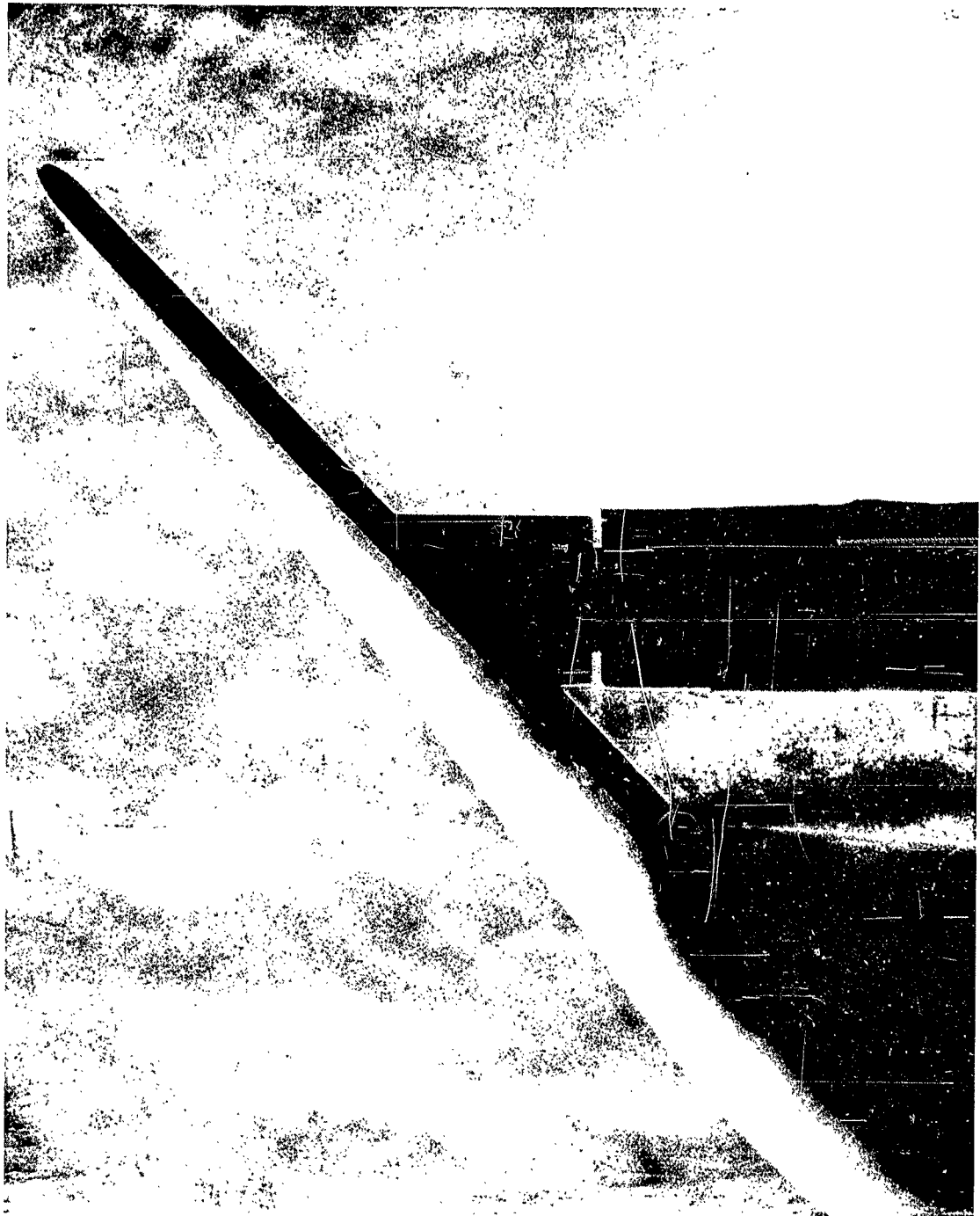
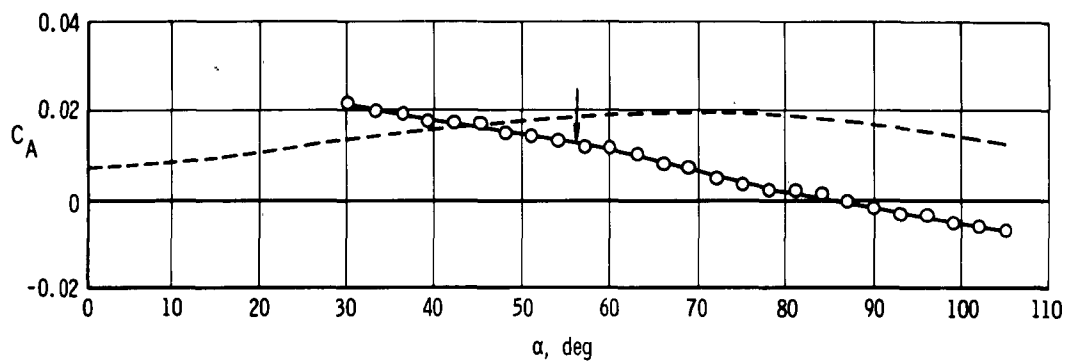
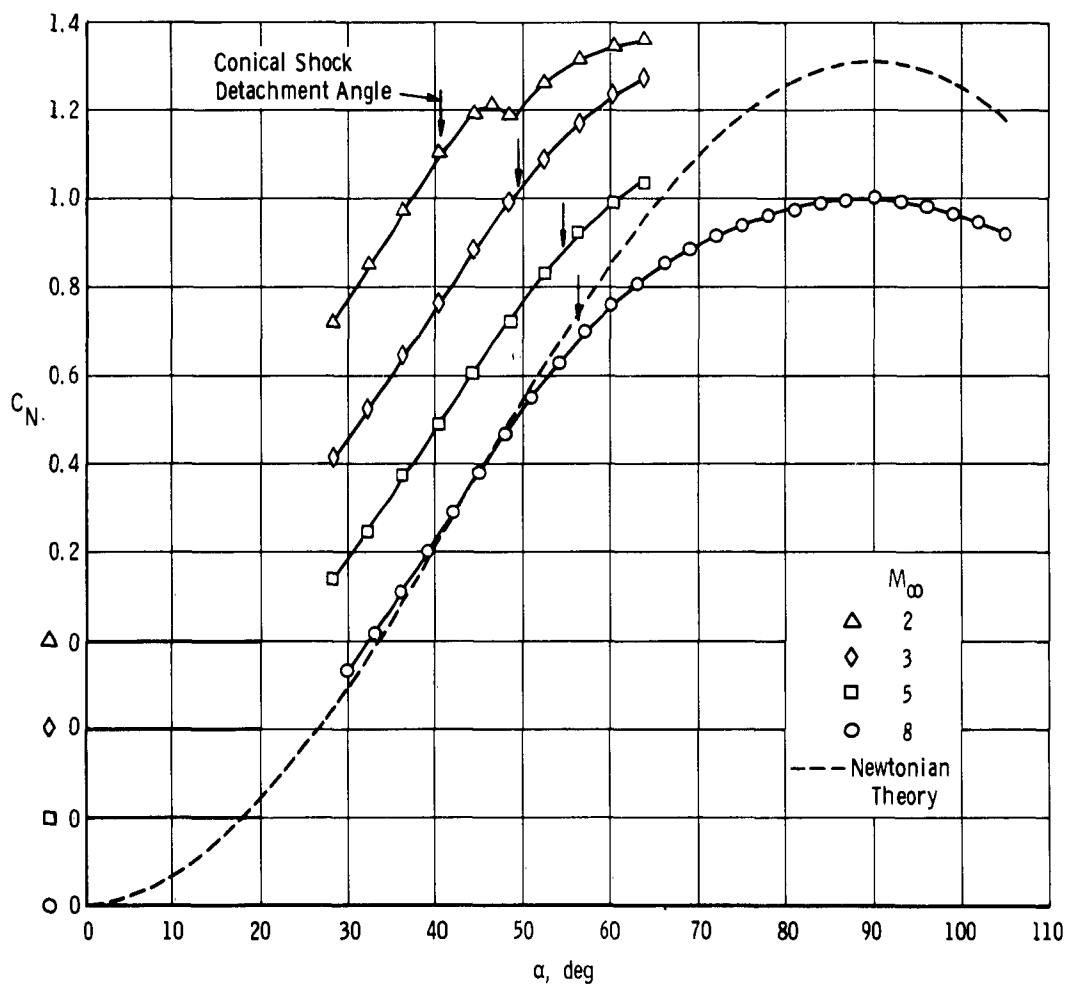


Fig. 5 Schlieren Picture of the Model at  $M_\infty = 5$  and  $\alpha = 45$  deg



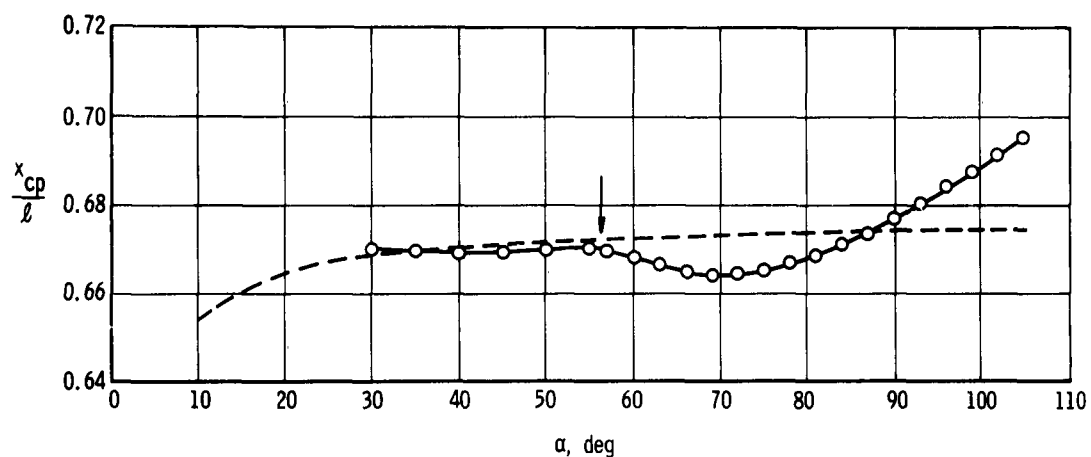
a. Axial Force,  $M_\infty = 8$



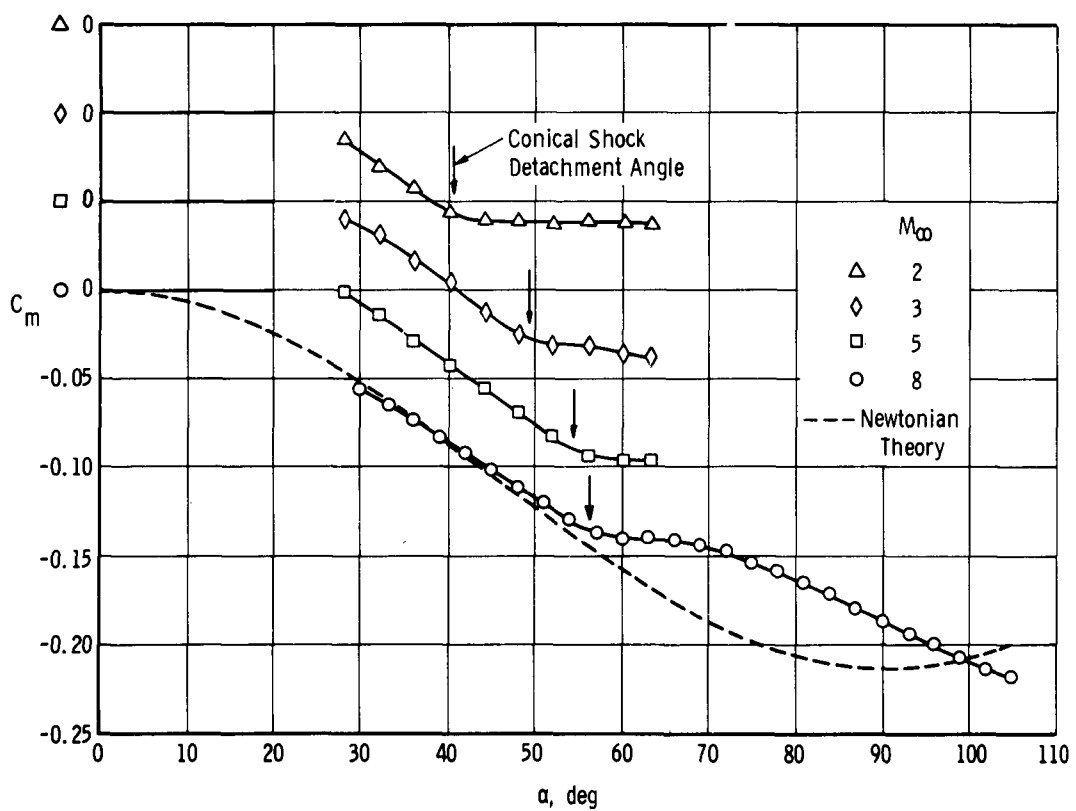
b. Normal Force

Fig. 6 Longitudinal Stability and Drag Characteristics



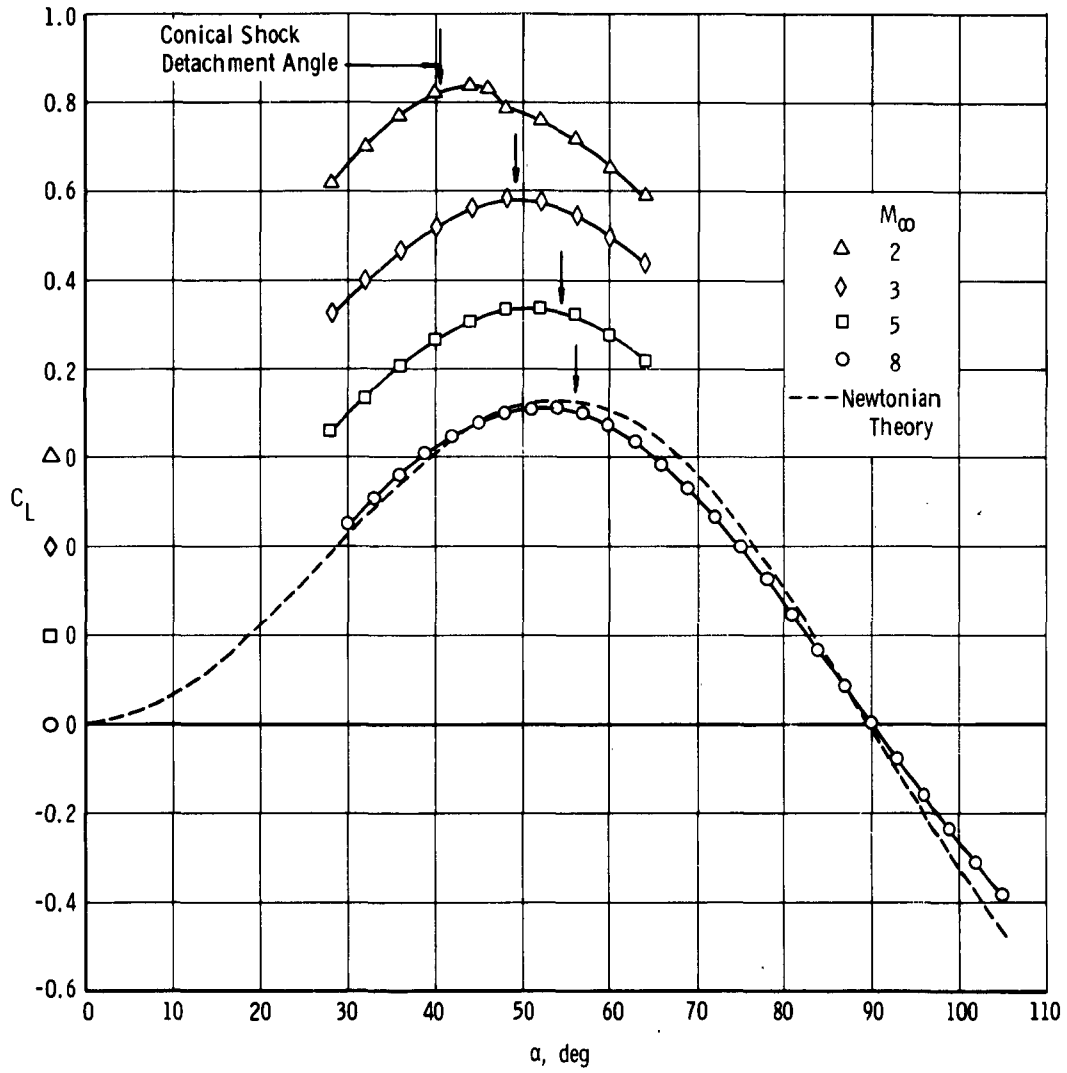


c. Center of Pressure,  $M_\infty = 8$



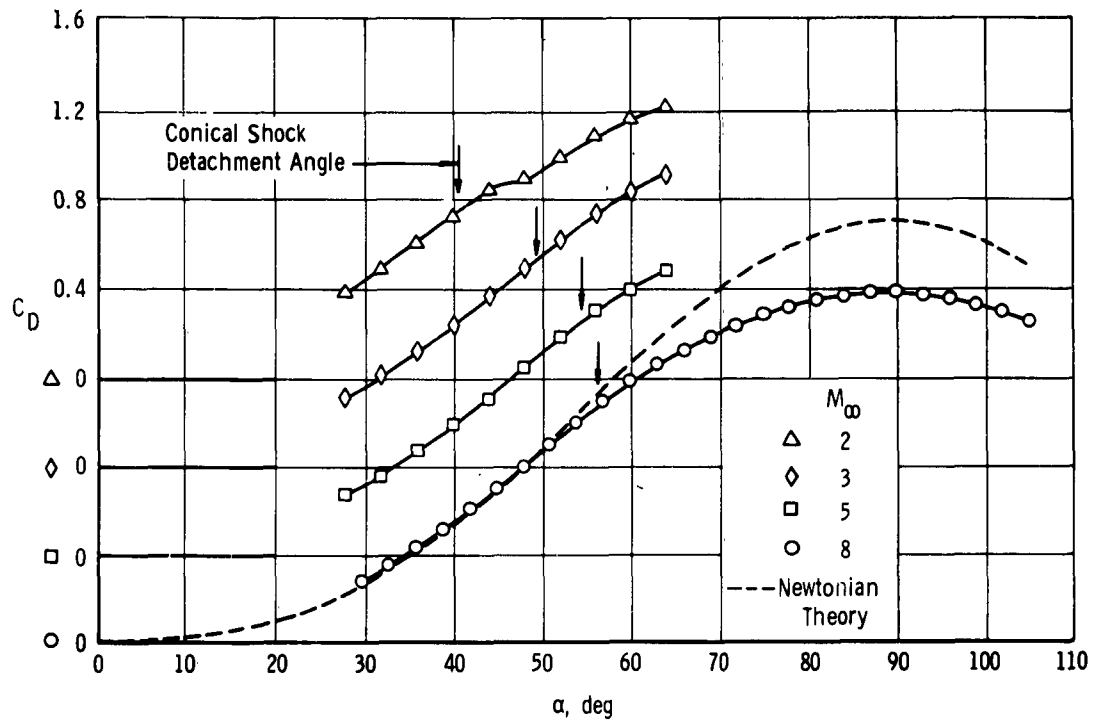
d. Pitching Moment

Fig. 6 Continued

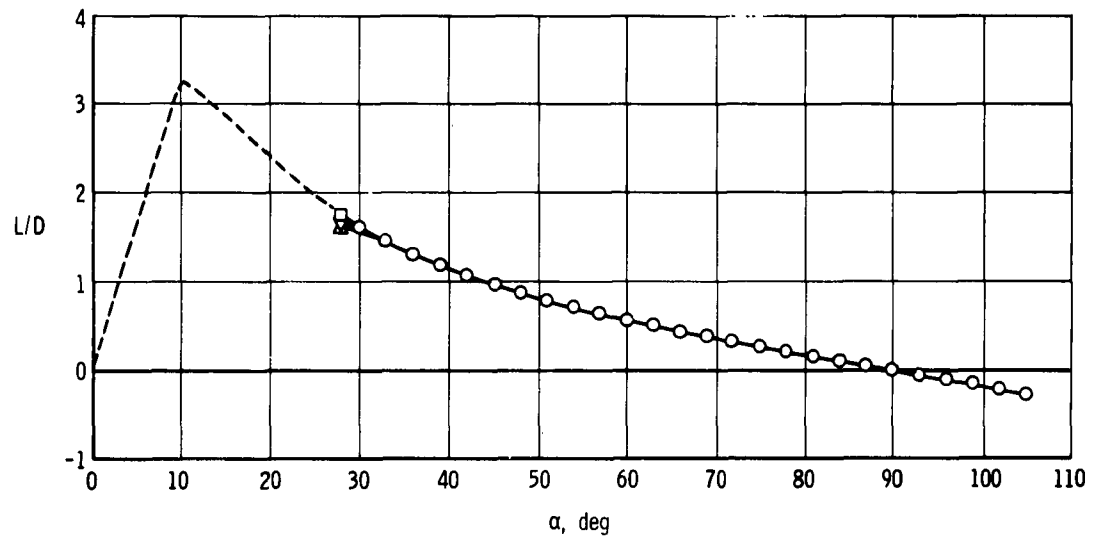


e. Lift

Fig. 6 Continued



f. Drag



g. Lift-to-Drag Ratio

Fig. 6 Concluded

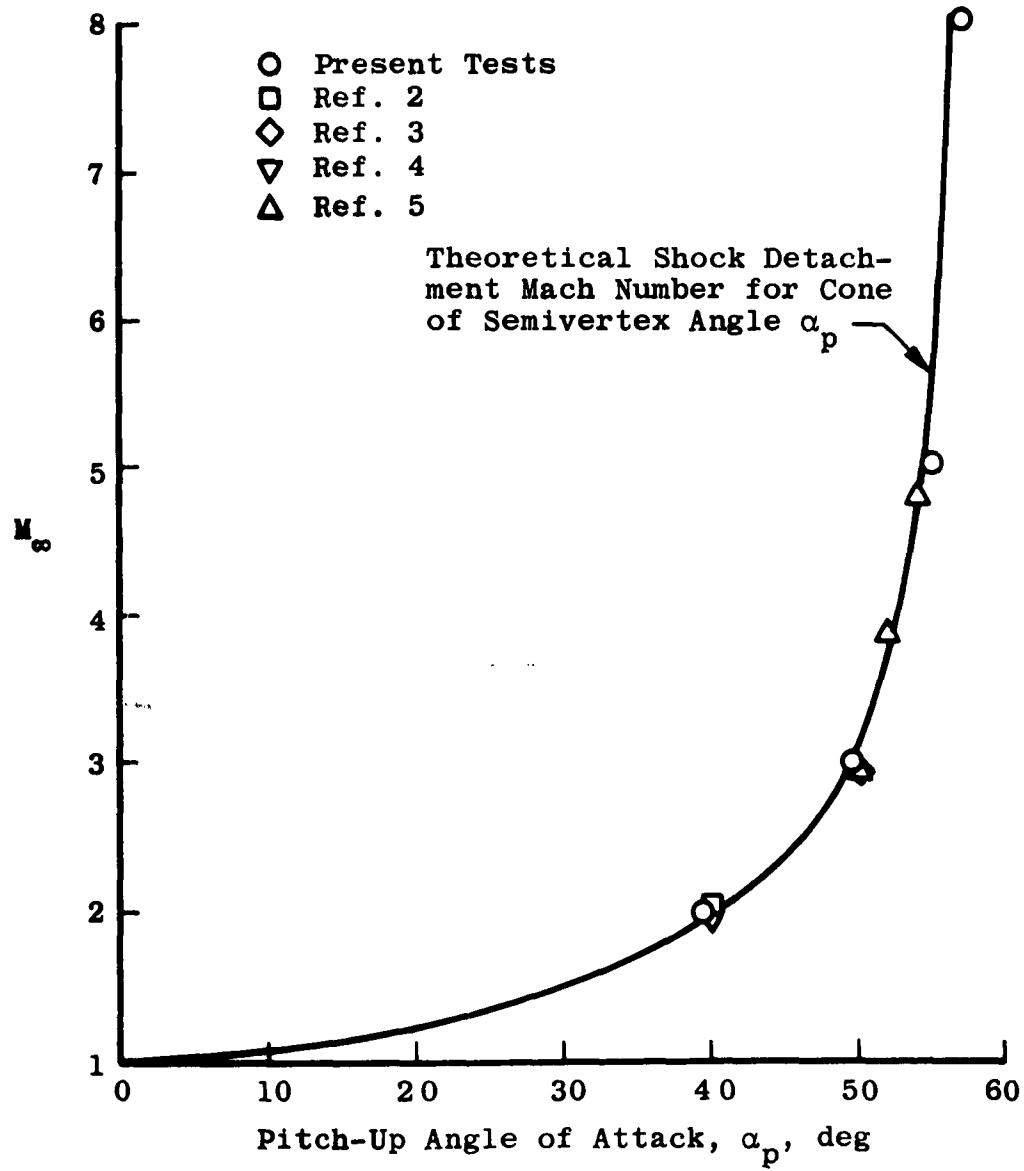


Fig. 7 Effect of Mach Number on the Pitch-Up Angle of Attack

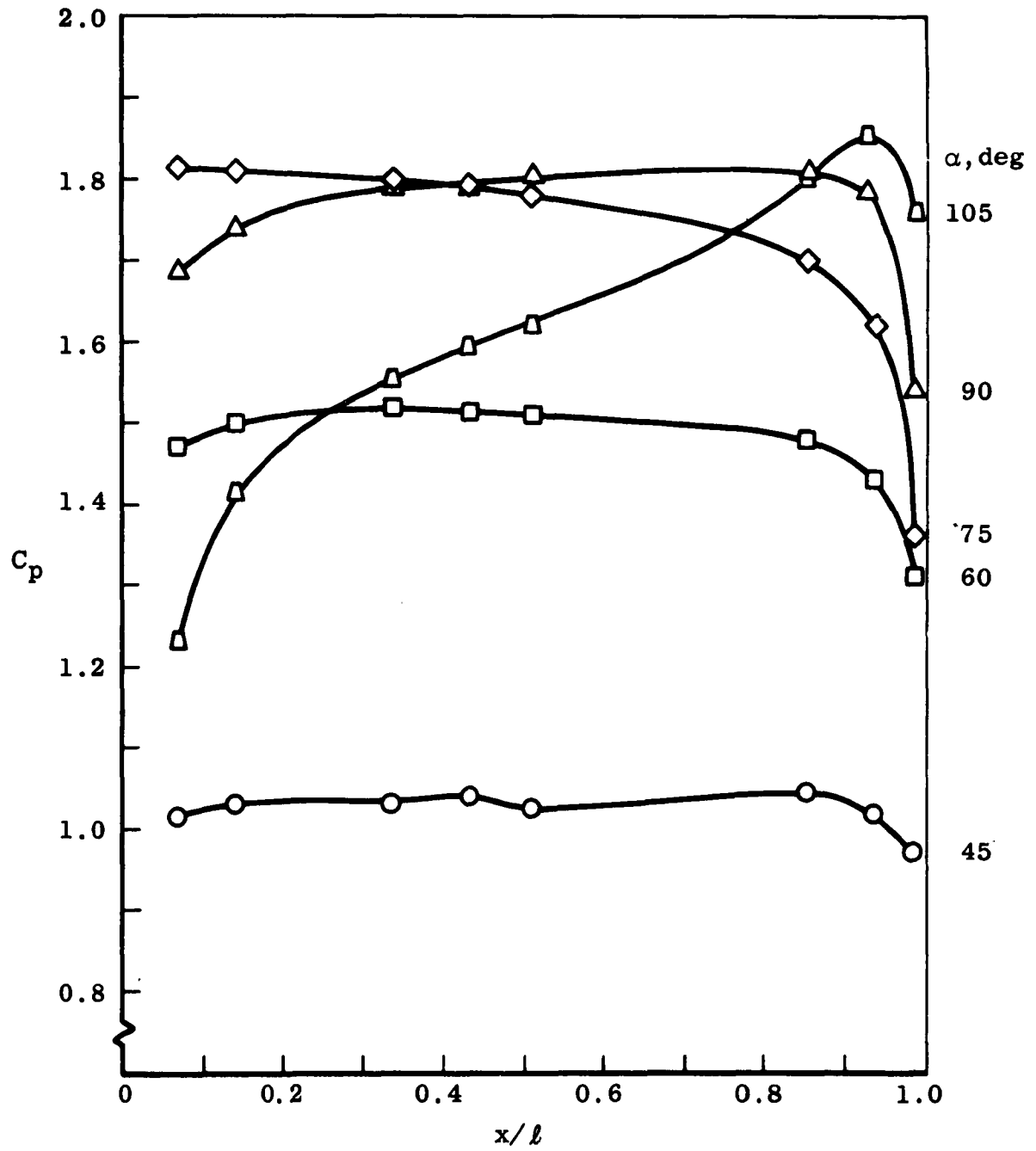


Fig. 8 Pressure Distribution on Model Centerline,  $M_\infty = 8$

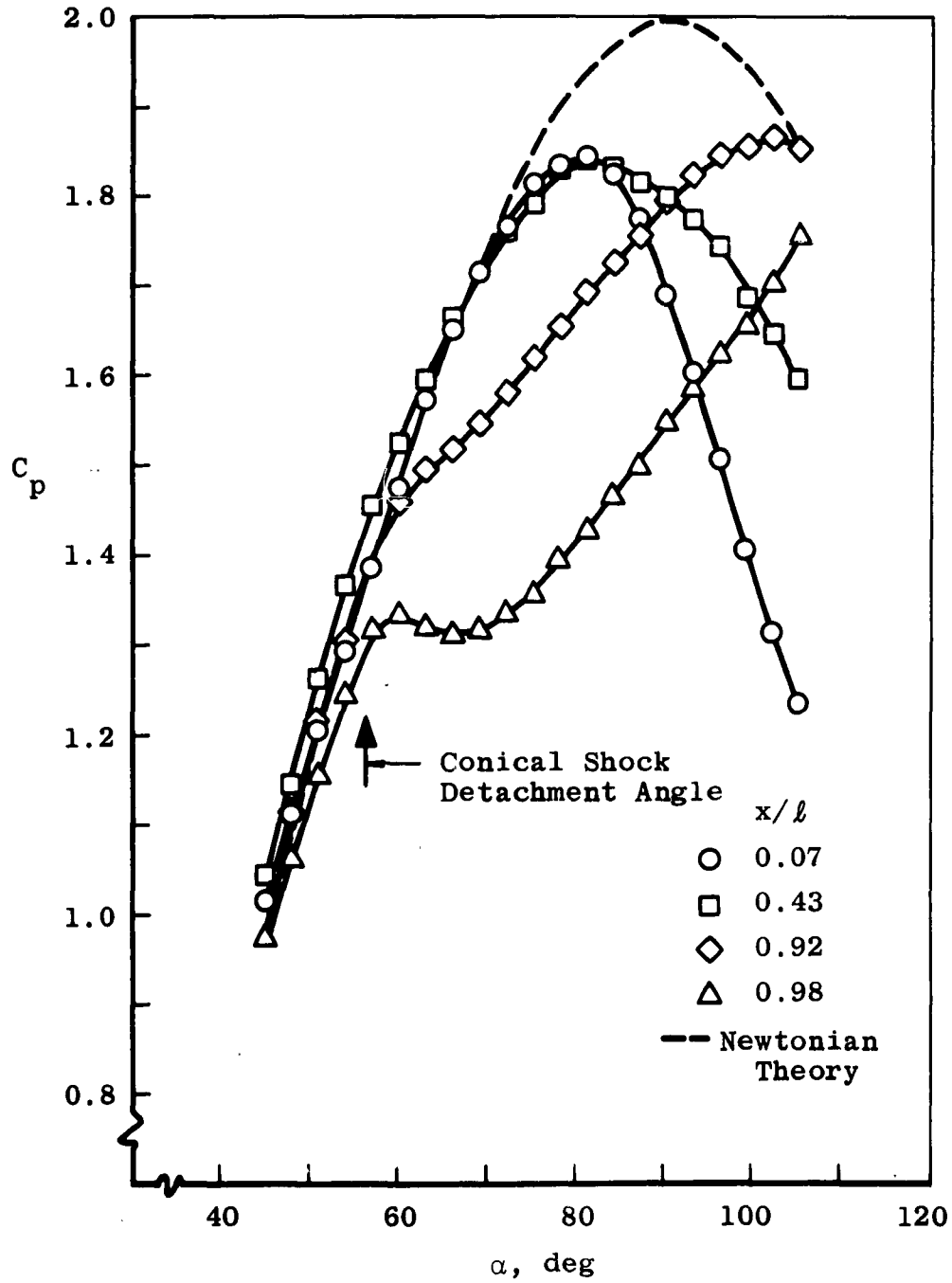


Fig. 9 Effect of Angle of Attack on Centerline Pressure,  $M_\infty = 8$

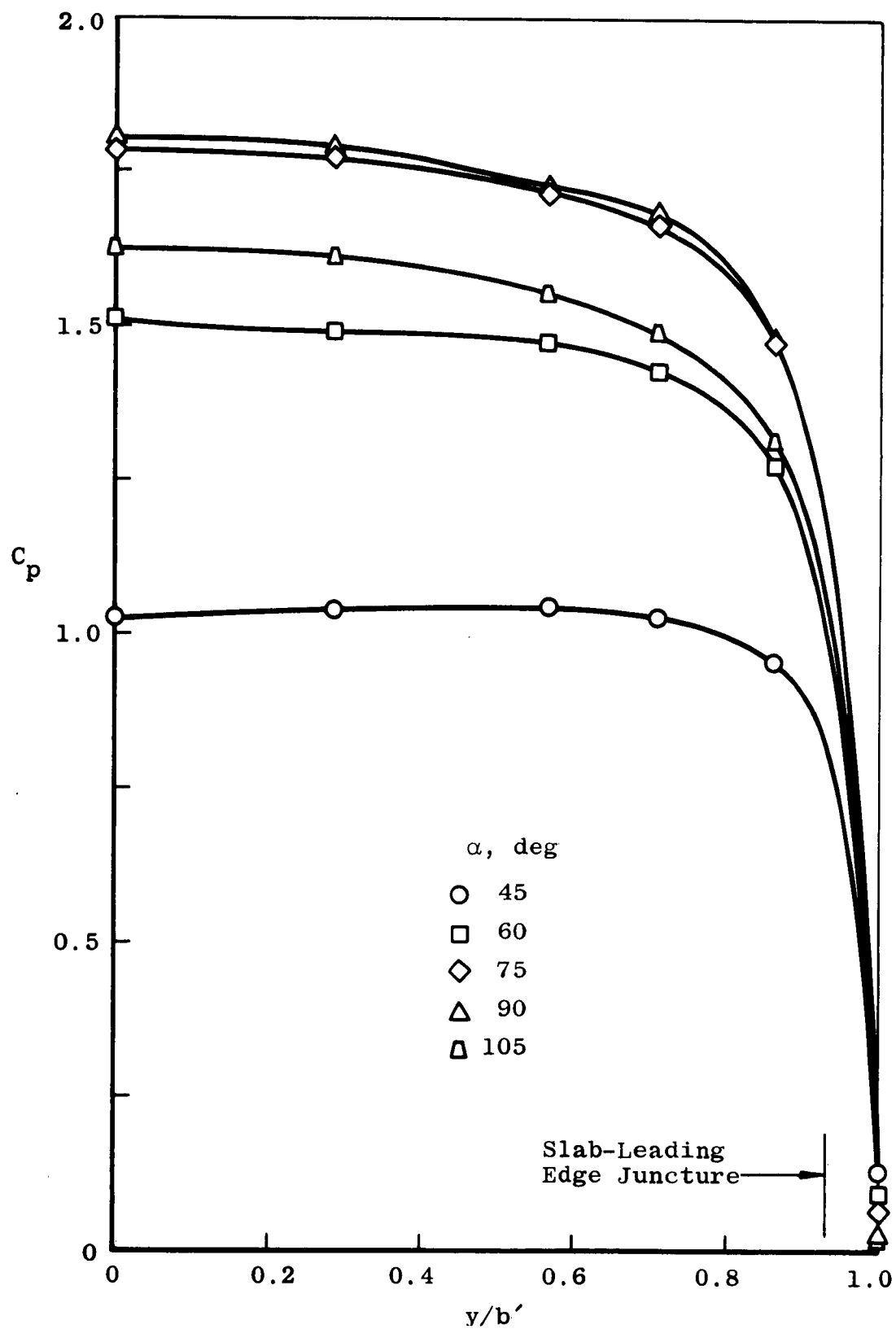


Fig. 10 Lateral Pressure Distribution at  $x/l = 0.51$ ,  $M_\infty = 8$

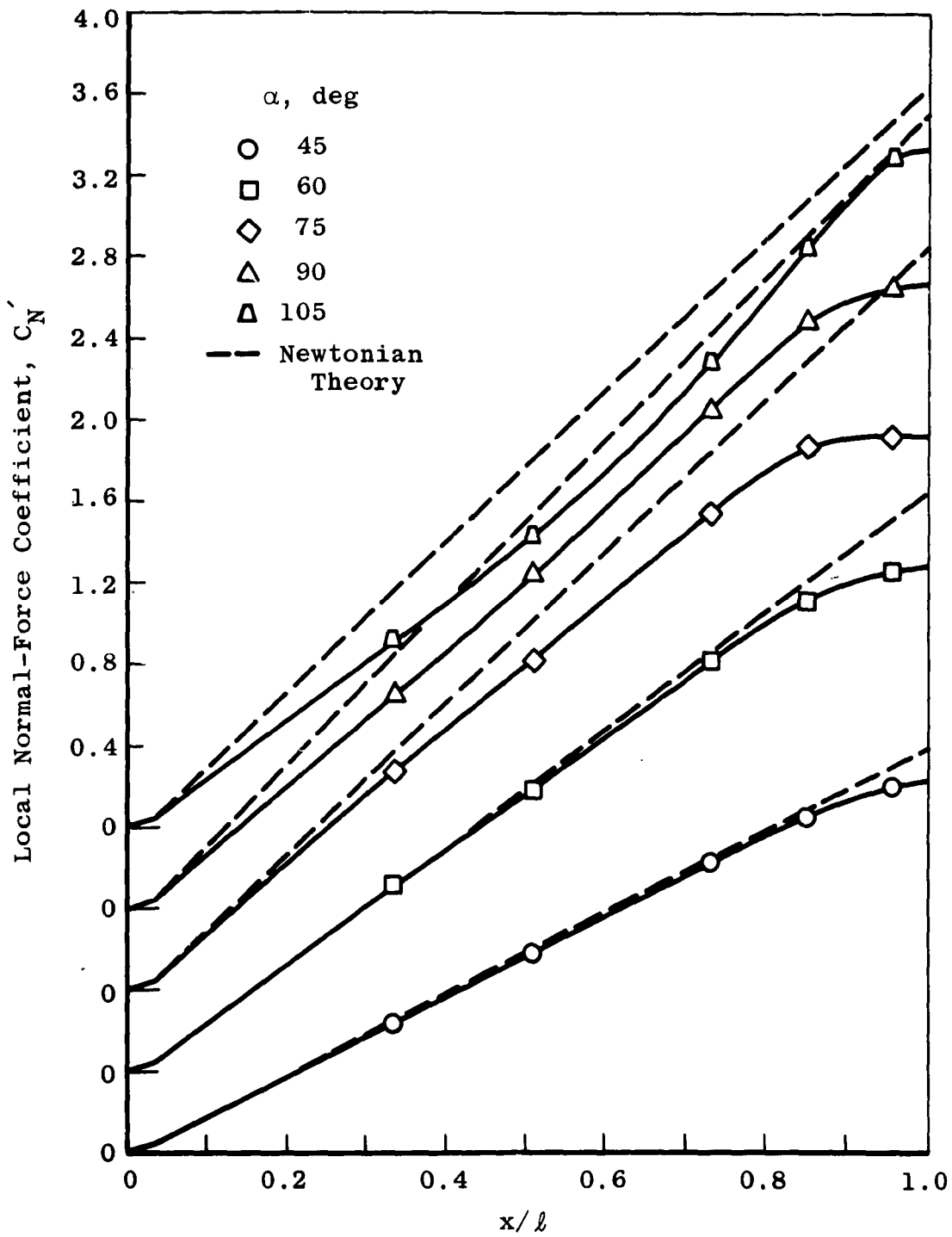
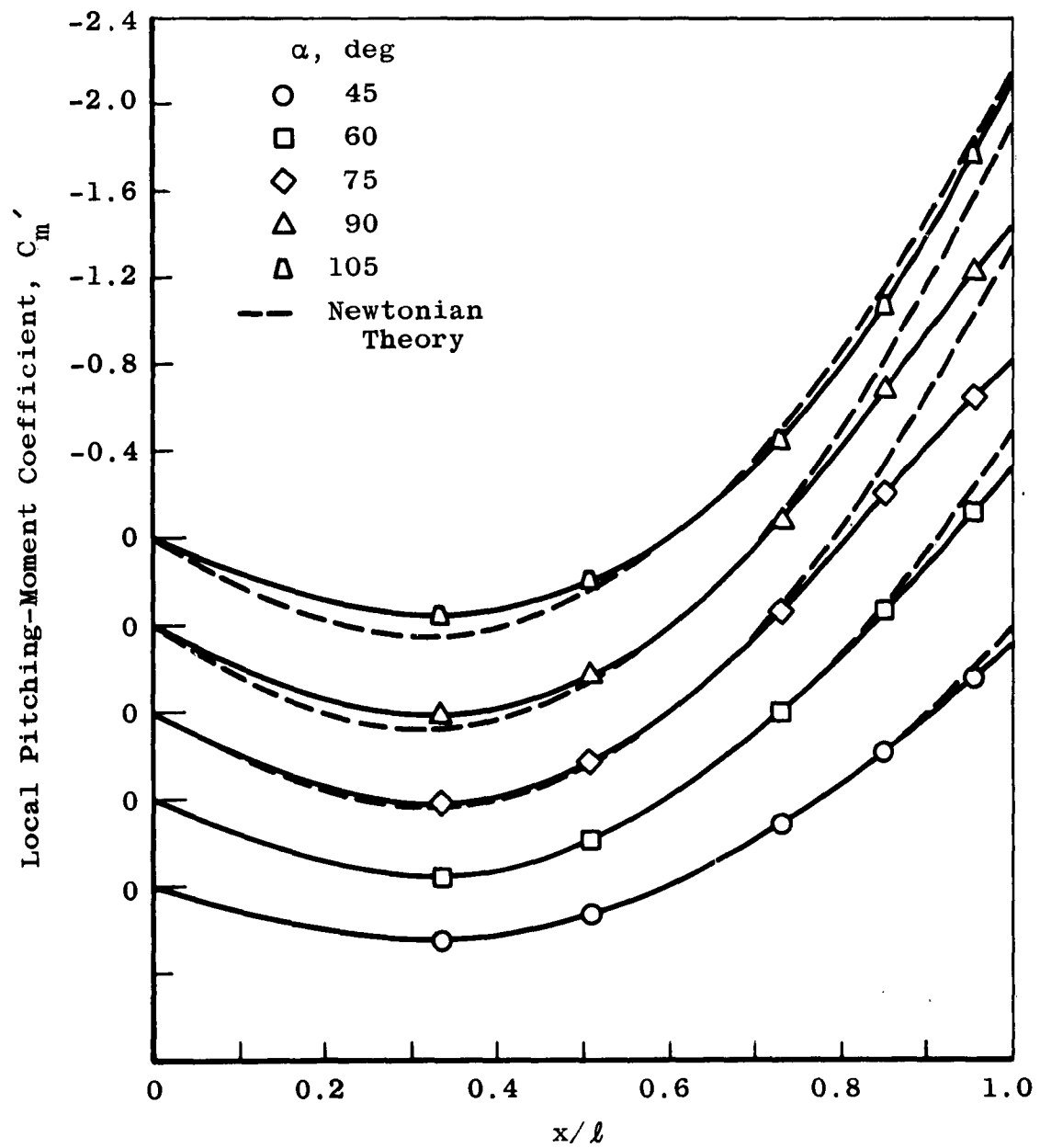


Fig. 11 Local Normal-Force Distribution,  $M_\infty = 8$



Fig. 12 Local Pitching-Moment Distribution,  $M_\infty = 8$

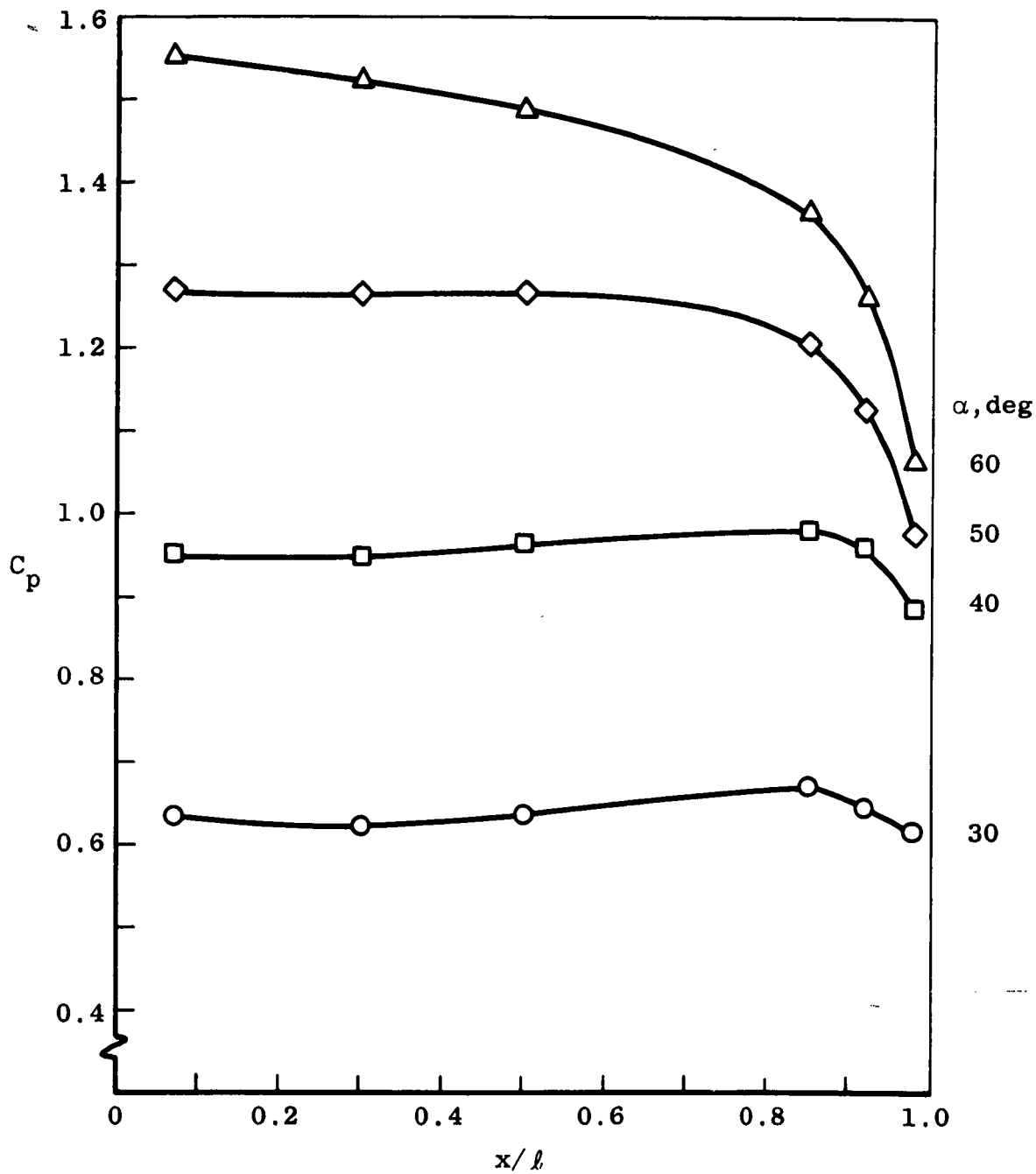


Fig. 13 Pressure Distribution on Model Centerline,  $M_\infty = 2$

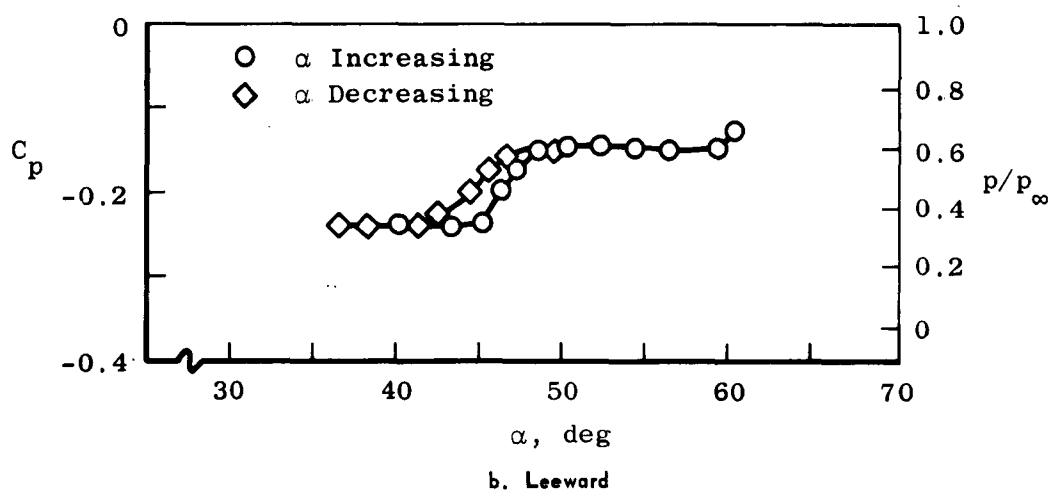
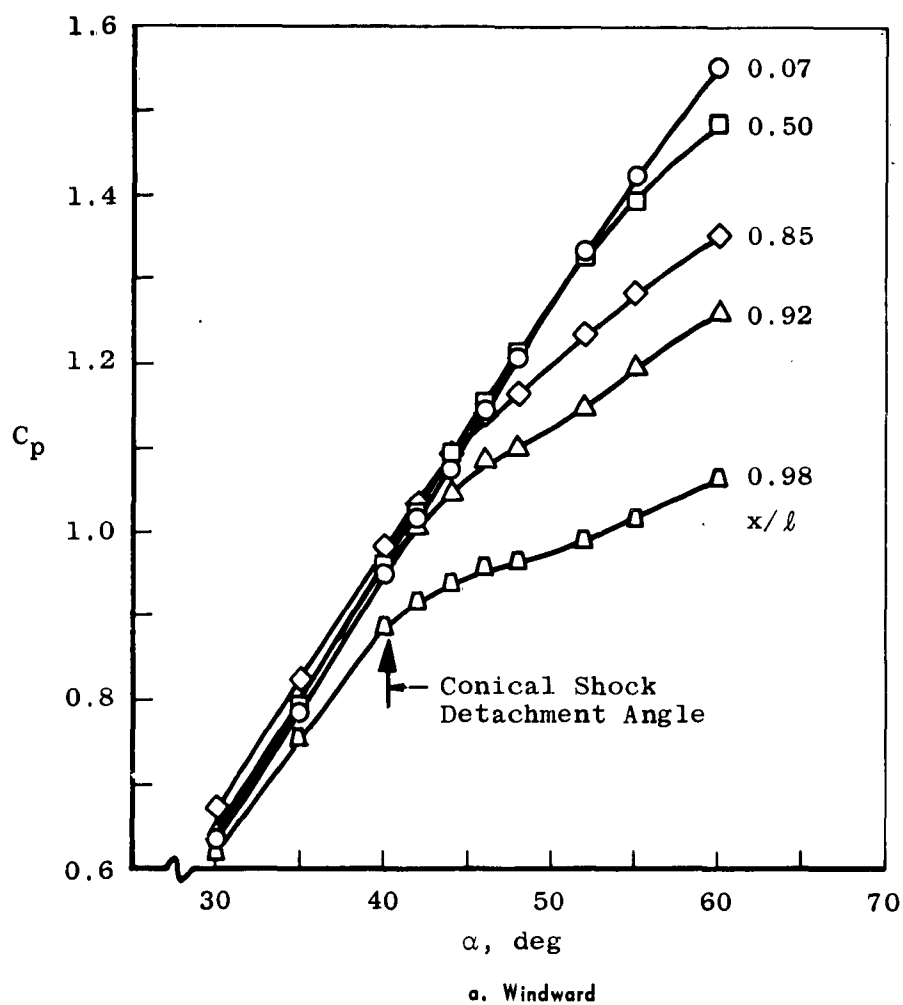
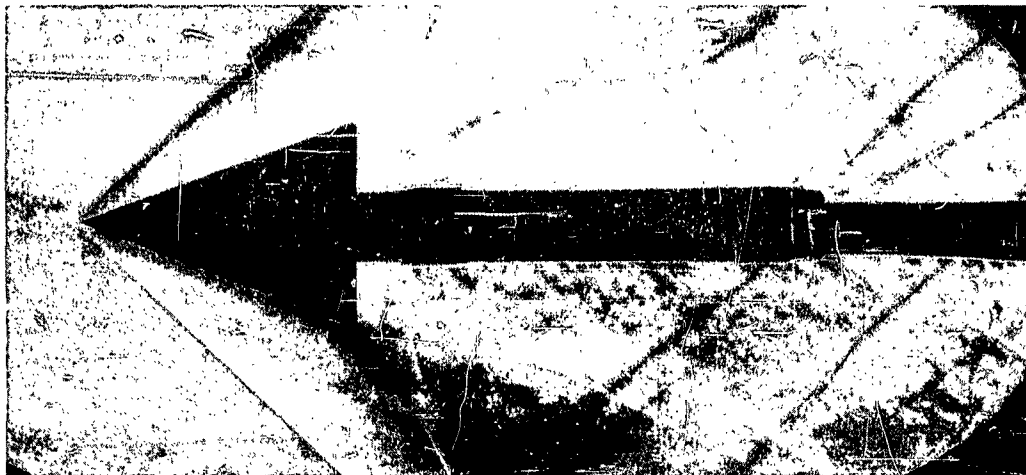
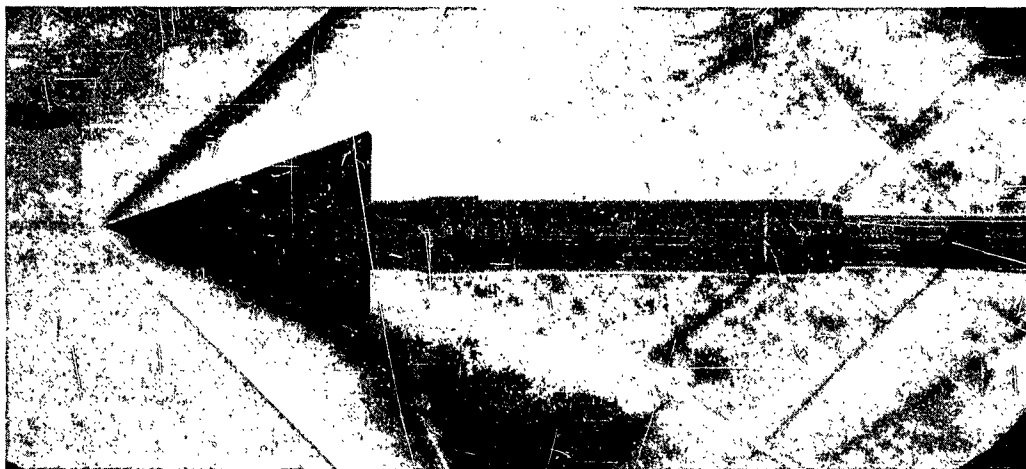


Fig. 14 Effect of Angle of Attack on Centerline Pressure,  $M_\infty = 2$

**CONFIDENTIAL**



$\alpha = 43^\circ$








$\alpha = 45^\circ$



$\alpha = 47^\circ$

Fig. 15 Schlieren Pictures of the Wake Geometry at  $M_\infty = 2$

**CONFIDENTIAL**

<p>Arnold Engineering Development Center Arnold Air Force Station, Tennessee</p> <p>Rpt. No. AEDC-TDR-62-99. THE AERODYNAMIC CHARACTERISTICS OF A 75-DEG SWEEP DELTA WING AT HIGH ANGLES OF ATTACK AND MACH NUMBERS OF 2 TO 8 (U). May 1962. 34 p. incl 8 refs., illus. Confidential Report</p> <p>An experimental investigation has been conducted in the 12-in. Supersonic Tunnel and the 50-in. Mach 8 Tunnel of the von Kármán Gas Dynamics Facility to determine the aerodynamic characteristics of a delta wing at high angles of attack. The configuration tested was a flat, blunt leading edge, delta wing with 75-deg sweepback. The tests were conducted at angles of attack from 30 to 105 deg and Mach numbers of 2, 3, 5, and 8. Longitudinal stability and drag characteristics, surface pressure distributions, and shock wave shapes are presented with theoretical estimates based on the Newtonian theory.            Unclassified Abstract</p>	<ol style="list-style-type: none"> <li>1. Triangular wings</li> <li>2. Aerodynamics</li> <li>3. Supersonics</li> <li>4. Swept back wings</li> <li>5. Pressure</li> <li>6. Tests</li> <li>7. Stability</li> <li>8. Load distribution</li> <li>9. Drag</li> </ol> <ol style="list-style-type: none"> <li>I. AFSC Program Area 750A, Project 8952</li> <li>II. Contract AF 40(600)-800 S/A 24(61-73)</li> <li>III. ARO, Inc., Arnold AF Sta, Tenn.</li> <li>IV. E. L. Clark and C. J. Spurlin</li> <li>V. In ASTIA collection</li> </ol>	<p>Arnold Engineering Development Center Arnold Air Force Station, Tennessee</p> <p>Rpt. No. AEDC-TDR-62-99. THE AERODYNAMIC CHARACTERISTICS OF A 75-DEG SWEEP DELTA WING AT HIGH ANGLES OF ATTACK AND MACH NUMBERS OF 2 TO 8 (U). May 1962. 34 p. incl 8 refs., illus. Confidential Report</p> <p>An experimental investigation has been conducted in the 12-in. Supersonic Tunnel and the 50-in. Mach 8 Tunnel of the von Kármán Gas Dynamics Facility to determine the aerodynamic characteristics of a delta wing at high angles of attack. The configuration tested was a flat, blunt leading edge, delta wing with 75-deg sweepback. The tests were conducted at angles of attack from 30 to 105 deg and Mach numbers of 2, 3, 5, and 8. Longitudinal stability and drag characteristics, surface pressure distributions, and shock wave shapes are presented with theoretical estimates based on the Newtonian theory.            Unclassified Abstract</p>	<ol style="list-style-type: none"> <li>1. Triangular wings</li> <li>2. Aerodynamics</li> <li>3. Supersonics</li> <li>4. Swept back wings</li> <li>5. Pressure</li> <li>6. Tests</li> <li>7. Stability</li> <li>8. Load distribution</li> <li>9. Drag</li> </ol> <ol style="list-style-type: none"> <li>I. AFSC Program Area 750A, Project 8952</li> <li>II. Contract AF 40(600)-800 S/A 24(61-73)</li> <li>III. ARO, Inc., Arnold AF Sta, Tenn.</li> <li>IV. E. L. Clark and C. J. Spurlin</li> <li>V. In ASTIA collection</li> </ol>			
---	---	---	---	---	---	---